Supplementary Information (SI) for ChemComm.
This journal is © The Royal Society of Chemistry 2026

Supporting Information

Bionic construction of iron ion-specific porous adsorbents for mitigating iron toxicity across diverse organisms

Yingbo Song, Fuli Cai, Cheng Zhang, Doudou Cao, Yue Zheng, Jiarui Cao, Lu Luo, Sirui Li, Xinbo Li and Ye Yuan*

[a]Key Laboratory of Polyoxometalate and Reticular Material Chemistry of Ministry of Education, Northeast Normal University. Changchun 130012, China

Corresponding authors (email: yuany101@nenu.edu.cn)

Experimental Procedures

Text S1

Chemicals and materials

All the reagents and solvents were obtained commercially and used without further purification.

Text S2

Characterization

FT-IR spectra were obtained on the Nicolet IS50 Fourier transform infrared spectrometer. Powder X-ray diffraction (PXRD) was performed on a Bruker D8 QUEST diffractometer with Cu-Kα radiation. Solid-state. N_2 adsorption and desorption isotherms were measured at 77 K using an Autosorb iQ_2 adsorptometer. All samples were degassed at 100 °C for 10 h under vacuum before measurements. The specific surface areas were calculated from the adsorption data using the Brunauer−Emmett−Teller (BET) method, and the pore size distribution was calculated by the Density Function Theory (DFT) method. ^{13}C CP/MAS solid-state NMR spectra were performed on a Bruker Avance III model 400 MHz NMR spectrometer at a MAS rate of 5 kHz. Scanning electron microscope (SEM) was conducted on the JEOS JSM 6700. Transmission electron microscope (TEM) was obtained on a JEM-2100 with an accelerating voltage of 200 kV. X-ray photoelectron spectroscopy (XPS) measurements were conducted on an Escalab-MK II photoelectron spectrometer with Al Kα (1200 eV). Inductively coupled plasma mass spectrometry (ICP-MS) was carried out on a PerkinElmer Optima 3300DV. Thermo-gravimetric analysis (TGA) was recorded by a METTLER TOLEDO TGA/DSC 2 thermal analyzer under an air atmosphere at a heating rate of 10 °C min^{-1}. UV-Vis absorption spectra were conducted with a spectrophotometer

(Cary500, VARIAN, America). X-ray spectroscopy (EDX) images were obtained on a Tecnai G2 F20 S-TWIN electron microscope (USA).

Text S3

Complexes synthesis

To construct a biomimetic binding site, a variety of carboxylic acid ligands was selected including vinylbenzoic acid (0.3 mmol, 45.36 mg), 4-pentenoic acid (0.3 mmol, 30.04 mg), and 1-allyl-3-methyl-1H-pyrazole-5-carboxylic acid (0.3 mmol, 49.85 mg). After pourding the acid ligands, $FeCl_3$ (0.1 mmol, 16.23 mg) was added to a flask containing 3 mL of 2-methoxyethanol. Stirred at room temperature for 24 h, the solvent was removed by vacuum heating at 110 °C to obtain Fe^{3+} ion-imprinted complexes with tricarboxylic acid.

Text S4

MIPAF synthesis

Preparation of porous networks via Heck coupling reactions. 1,3,5-tris(4-bromophenyl)benzene (0.267 mmol, 144.83 mg), Fe^{3+} imprinted complexes, p-divinylbenzene, K_2CO_3 (1 mmol, 138.21 mg) were sequentially added to a 50 mL double-necked round-bottomed flask and the amount of imprinted complex ranges from 0% to 25%, 30%, and 40%, respectively. Subsequently, 15 mL of anhydrous DMF and tetrakis(triphenylphosphine)palladium (Pd_0) (0.0129 mmol, 15 mg) were added. The flask were then rapidly frozen at 77 K (liquid nitrogen bath) and degassed by three freeze-pump evacuation-thaw cycles. Thermally polymerized in an oil bath at 80 °C while stirring for 48 h and then elevated to 120 °C with stirring for 72 h. The products were collected and washed with $CHCl_3$, methanol, and acetone, respectively, and then filtered. The sdproducts were collected by filtration and extracted by Soxhlet extraction with $CHCl_2$ for 36 h. After vacuum drying at 100 °C, products were obtained as PAF-0%, PAF-25%, PAF-30% and PAF-40%, respectively. The obtained PAFs materials were stirred with NaOH (1 mol L^{-1}) and HCl (1 mol L^{-1}) solutions sequentially for 6 h for the elution of Fe^{3+} ion, and finally collected by filtration under vacuum to obtain the dried MIPAF-0%, MIPAF-25%, MIPAF-30%, and MIPAF-40%.

Text S5

NIPAF synthesis

$FeCl_3$ (0.1 mmol, 16.23 mg), 4-vinylbenzoic acid (0.3 mmol, 45.36 mg), 1,3,5-tris(4-bromophenyl)benzene (0.267 mmol, 144.83 mg), *p*-divinylbenzene (0.3 mmol, 53.2 μL) and K_2CO_3 (1 mmol, 138.21 mg) were sequentially added to a 50 mL double-necked round-bottomed flask. Subsequently, 15 mL of anhydrous DMF and Pd_0 (0.0129 mmol, 15 mg) were added. The flask was then rapidly frozen at 77 K (liquid nitrogen bath) and degassed by three freeze-pump evacuation-thaw cycles. Thermally polymerized in an oil bath at 80 °C while stirring for 48 h and then elevated to 120 °C with stirring for 72 h. Thermally polymerized in an oil bath at 80 °C while stirring for 48 h and then elevated to 120 °C with stirring for 72 h. The products were collected and washed with $CHCl_3$, and THF, respectively, and then filtered. The products were collected by filtration and extracted by Soxhlet extraction with $CHCl_2$ for 36 h. After vacuum drying at 100 °C, grey-green products were obtained as PAF-0%, PAF-25%, PAF-30%, and PAF-40%, respectively. The final NIPAF is obtained by drying at 100 °C.

Text S6

Iron adsorption capacity

$FeCl_3$ (0.12 mmol, 20 mg) was weighed in a 250 mL beaker and configured as a 20 ppm solution of Fe^{3+} in a 1 L volumetric flask with deionised water. Subsequently, 2 mg of each of the different proportions of the material was weighed into 200 mL of the above solution and stirred at room temperature. The supernatant was filtered through a 0.45 μm membrane filter at 0, 0.1, 0.25, 1, 4, 6, 12, and 24 h. The concentration of iron ions was determined by inductively coupled plasma mass spectrometer (ICP-MS).

The adsorption of iron ions was calculated by the following equation:

$$q_e = \frac{(C_0 - C_e) \times V}{m}$$

q_e is the equilibrium saturation capacity adsorption value (mg g^{-1});

C_0 is the initial concentration (ppm);

C_e is the equilibrium concentration (ppm);

V is the adsorption volume (L);

m is the mass of input adsorption material (g).

Text S7

Iron ion adsorption kinetics

In order to analyse the main adsorption modes of the adsorbent, two kinetic models fitted with linear expressions were used to study the adsorption kinetics of Fe^{3+} ion on the adsorbent. The *pseudo-first-order* kinetic model assumes that adsorption is controlled by a diffusion step. In contrast, the *pseudo-second-order* kinetic model assumes that adsorption is controlled by chemisorption.

The *pseudo-first-order* kinetic model is calculated as follows:

$$\log (Q_e - Q_t) = \log Q_e - \frac{k_1}{2.303} t$$

The *pseudo-second-order* kinetic model is calculated as follows:

$$\frac{t}{Q_t} = \frac{1}{k_2 \times Q_e^2} + \frac{1}{Q_e} t$$

Q_t (mg g^{-1}) is the adsorption capacity at time t (h), respectively;

Q_e (mg g^{-1}) are the adsorption capacities at equilibrium at time t (h), respectively;

k_1 is the kinetic adsorption rate constant for the *pseudo-first-order* kinetic model;

k_2 is the kinetic adsorption rate constant of the *pseudo-second-order* kinetic model.

Text S8

Iron ion adsorption thermodynamics

The adsorbent was dispersed into different concentrations of ferric ion solutions with constant speed stirring at room temperature. The supernatant was extracted from the adsorbed solution and filtered through a 0.45 μm membrane filter to assess the adsorption capacity of Fe^{3+} ions. The adsorption curves were fitted by two equations, *Langmuir* and *Freundlich*.

The *Langmuir* model is calculated as follows:

$$\frac{C_e}{q_e} = \frac{1}{k_L q_{max}} + \frac{C_e}{q_{max}}$$

The *Freundlich* model is calculated as follows:

$$\ln q_e = \ln K_F + \frac{1}{n} C_e$$

C_e is the concentration of interfering ions at equilibrium (ppm);

q_e is the Fe^{3+} adsorption capacity of the adsorbent material (mg g^{-1});

q_m is the maximum Fe^{3+} adsorption capacity (mg g^{-1}) in the model;

k_L is the model parameter.

Text S9

Ion selectivity

$FeCl_3$ was calculated and configured to have a concentration of 20 ppm of Fe^{3+} ion, to which the same concentrations of Cu^{2+}, K^{+}, Ca^{2+}, Mg^{2+}, Co^{2+}, Zn^{2+}, Mn^{2+}, Sr^{2+}, and Li^{+} were added to form a 500 mL adsorbent system. 5 mg of adsorbent material was weighed and added to disperse homogeneously and stirred, and after saturation of adsorption, the change in the concentration of ferric ions was detected by ICP-MS and the formulae are as follows

$$K_{Fe/M} = \frac{Q_{Fe}}{Q_M} \times 100\%$$

Q_{Fe} is the amount of Fe^{3+} adsorbed (mg g^{-1});

Q_M is the amount of interfering metal adsorbed (mg g^{-1});

$K_{(Fe/M)}$ is the material selectivity correlation coefficient.

Cycle stability

The adsorbent after adsorption of iron is immersed in a 1 mol L^{-1} NaOH solution and stirred, and the iron adsorbed in the adsorbent can be desorbed. The regenerated adsorbent can be used in subsequent iron adsorption-desorption cycles.

Text S10

Adsorption experiments of adsorbents on six plant species

Each of six plants—salvia miltiorrhiza bunge (SB), gastrodia elata blume (GB), rheum officinale (RO), coptis, astragalus membranaceus (AM), and pleuropterus multiflorus (PM) (1.0 g) and HNO_3 (0.1 M, 10 mL) were added to a 50 mL conical bottle. After being stirred at room temperature for 24 h, 10 mL of HNO_3 (0.1 M) and 5 mL of $HClO_4$ (0.1 M) were added and stirred for 12 h at 60 ℃. When 1 mL of the solution remains, add 2 mL of HNO_3 (0.1 M) and 5 mL of $HClO_4$ (0.1 M), and stir for 10 h until the solution is colourless and transparent. Finally, transfer to a 200 mL volumetric flask, add water to the scale and mix thoroughly for subsequent experiments.

Text S11

Density functional theory (DFT) calculations

To gain deeper insights into the excellent iron ion sorption performance of MIPAFs and complexes, DFT calculations were carried out using Gaussian 16 software. The B3LYP functional was adopted for all calculations in combination with the D3BJ dispersion correction. For geometry optimization and frequency calculations, the def2TZVPP basis set was used for all atoms.

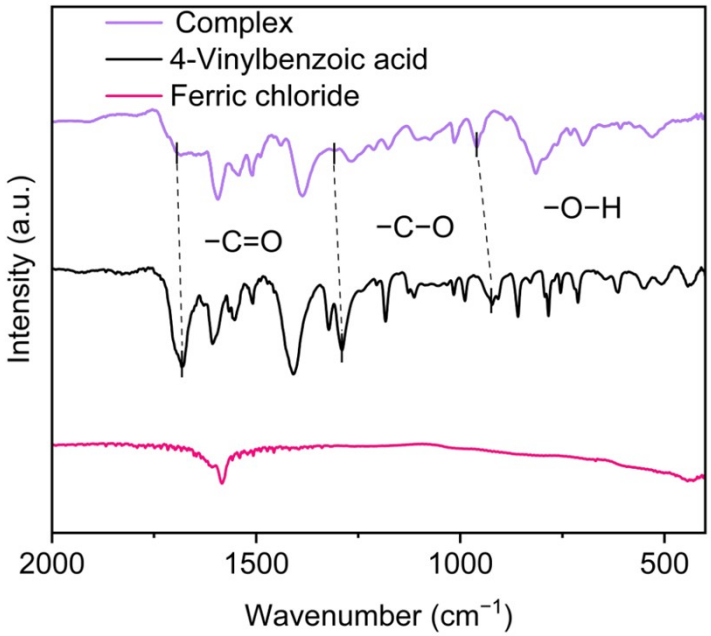

Fig. S1 FT-IR spectra for ion-coordinated complex, 4-vinyibenzoic acid, and ferric chloride.

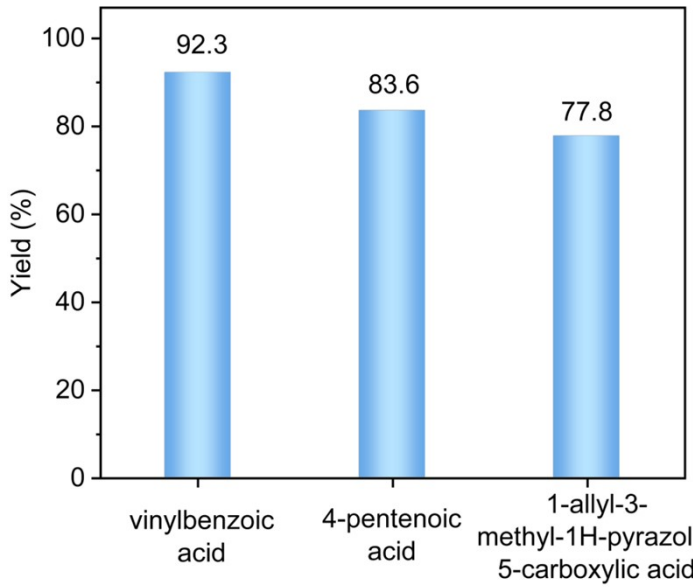

Fig. S2 Mass yield with different carboxylic acid monomers as Fe ion complexes.

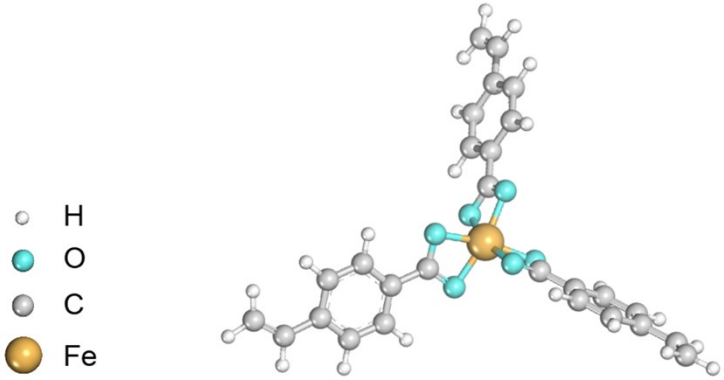

Fig. S3 Binding energy of the iron ion binding site.

According to density functional theory (DFT) calculations, the binding energy of the iron ion binding site formed by the vinylbenzoic acid ligand was −1401.5 kcal mol^{-1}.

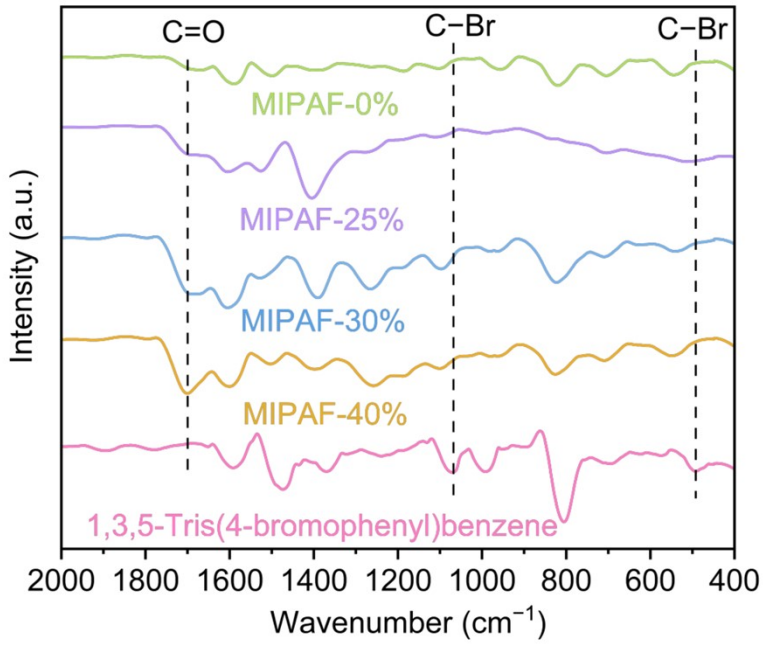

Fig. S4 FT-IR spectra for 1,3,5,-tris(4-bromophenyl)benzene and MIPAF-x (x = 0, 25%, 30% and 40%).

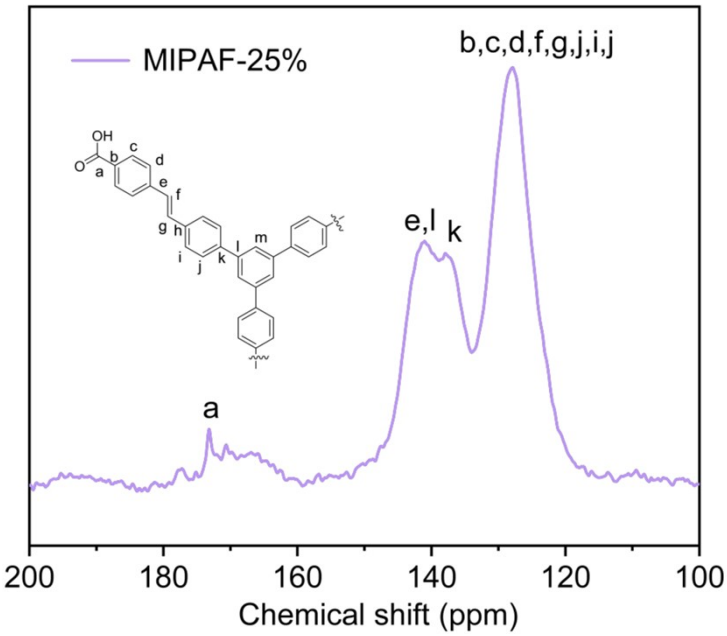

Fig. S5 Solid-state ^{13}C CP/MAS NMR spectra of MIPAF-25%.

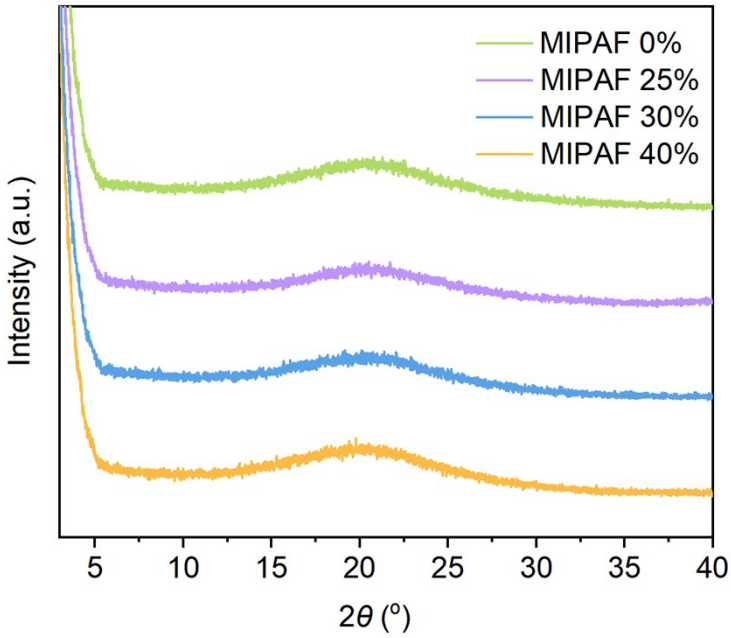

Fig. S6 PXRD patterns of MIPAF-0%, MIPAF-25%, MIPAF-30%, and MIPAF-40%.

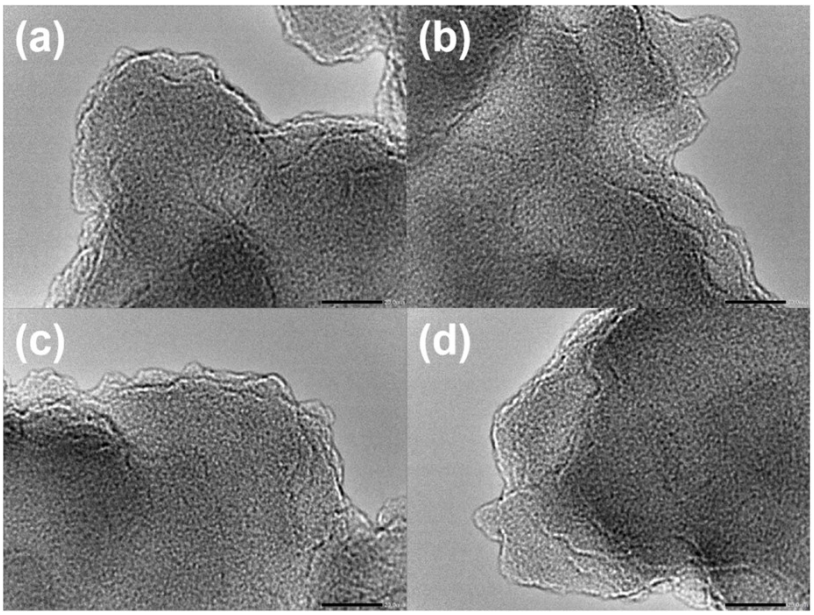

Fig. S7 TEM image of (a) MIPAF-0%, (b) MIPAF-25%, (c) MIPAF-30%, and (d) MIPAF-40%.

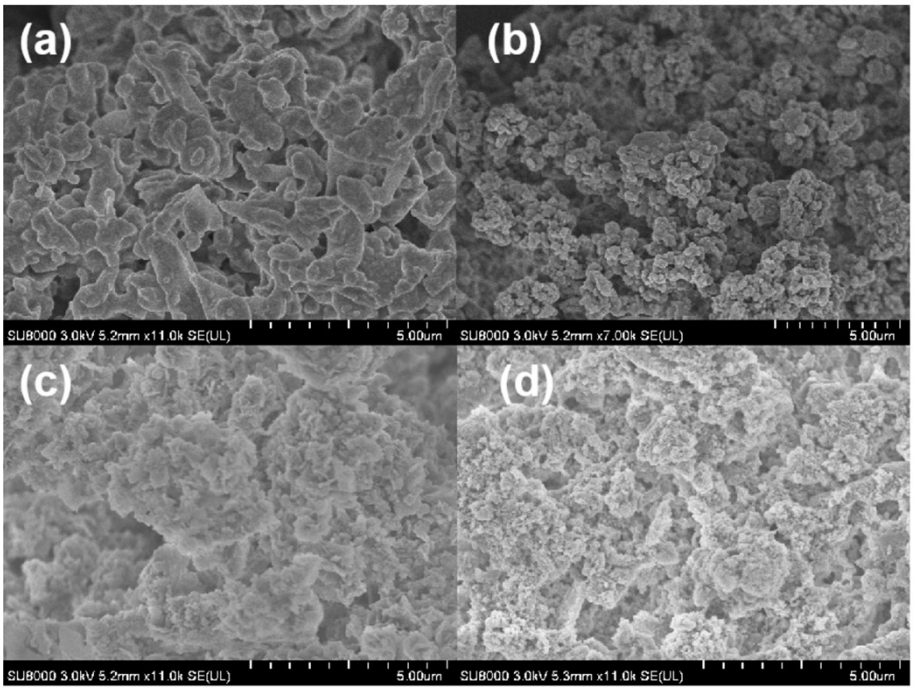

Fig. S8 SEM images for (a) MIPAF-0%, (b) MIPAF-25%, (c) MIPAF-30%, and (d) MIPAF-40%.

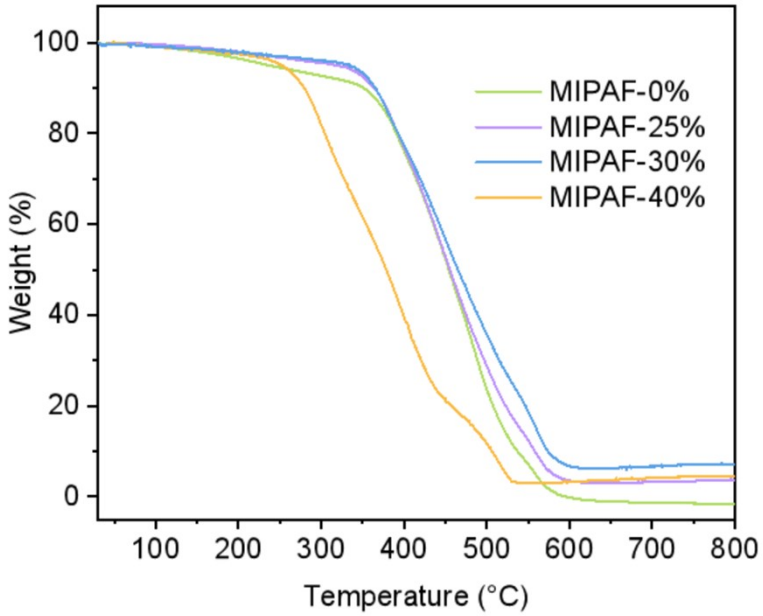

Fig. S9 TGA curves of MIPAF-x (x = 0, 25%, 30%, and 40%).

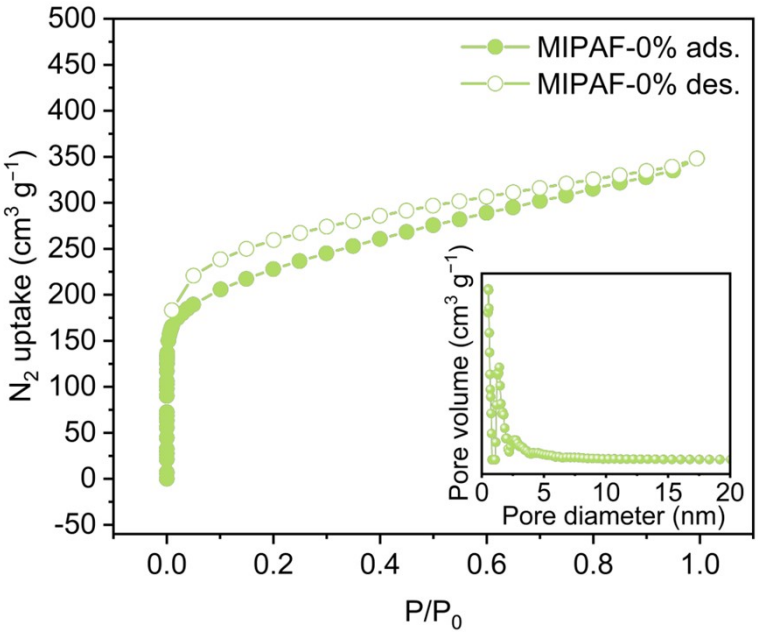

Fig. S10 Nitrogen adsorption-desorption isotherms and pore size distributions of MIPAF-0%.

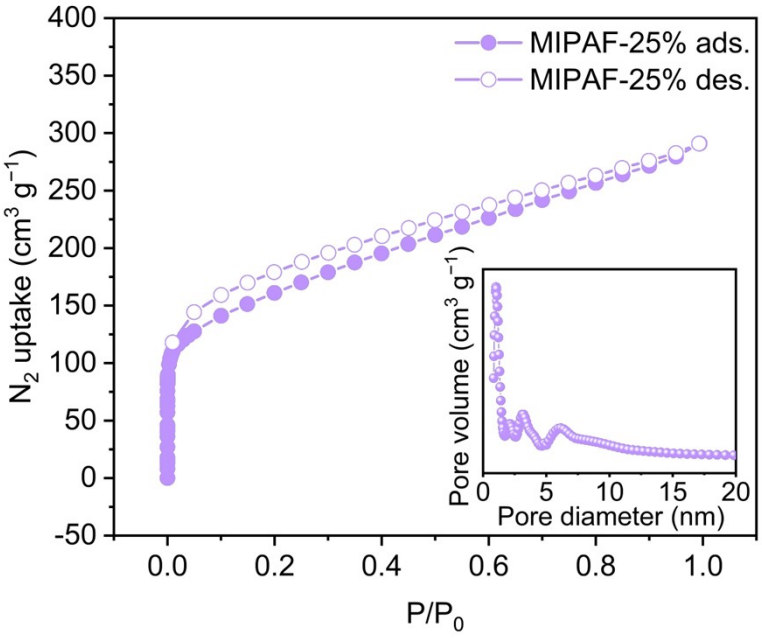

Fig. S11 Nitrogen adsorption-desorption isotherms and pore size distributions of MIPAF-25%.

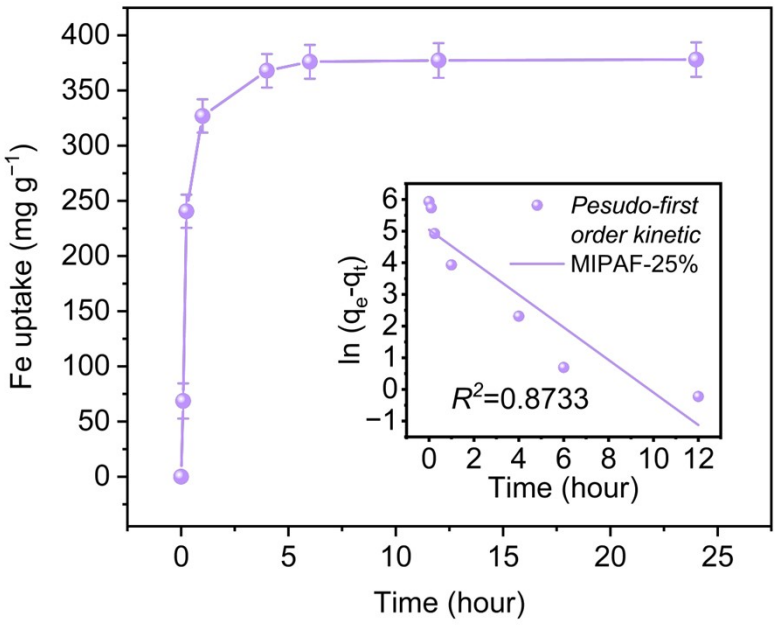

Fig. S12 Time-dependent uptake data using *pseudo-first-order.*

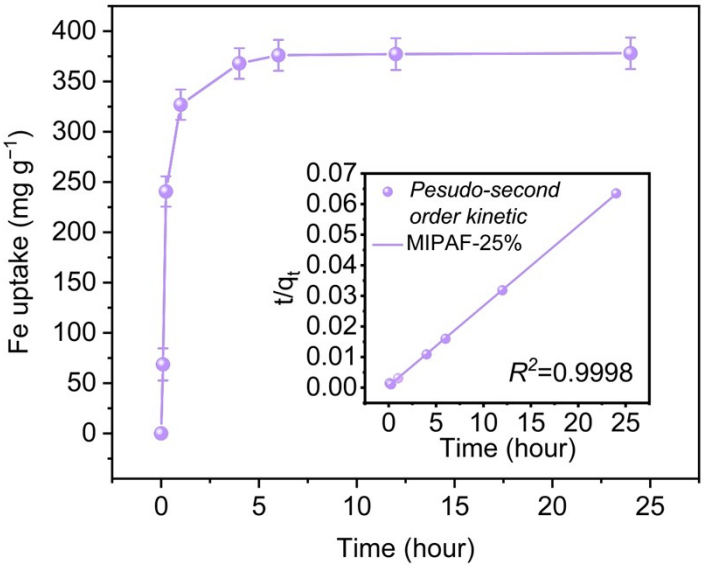

Fig. S13 Time-dependent uptake data using *pseudo-second-order.*

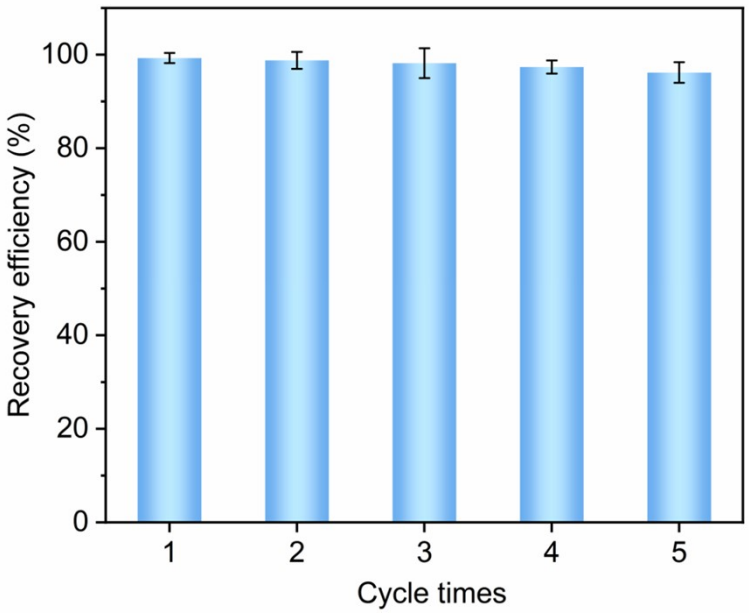

Fig. S14 Recycling experiment of MIPAF-25% in HCl solution (0.01 M).

After five consecutive cycles, the adsorption capacity of MIPAF-25% in HCl solution decreased by 3.8%.

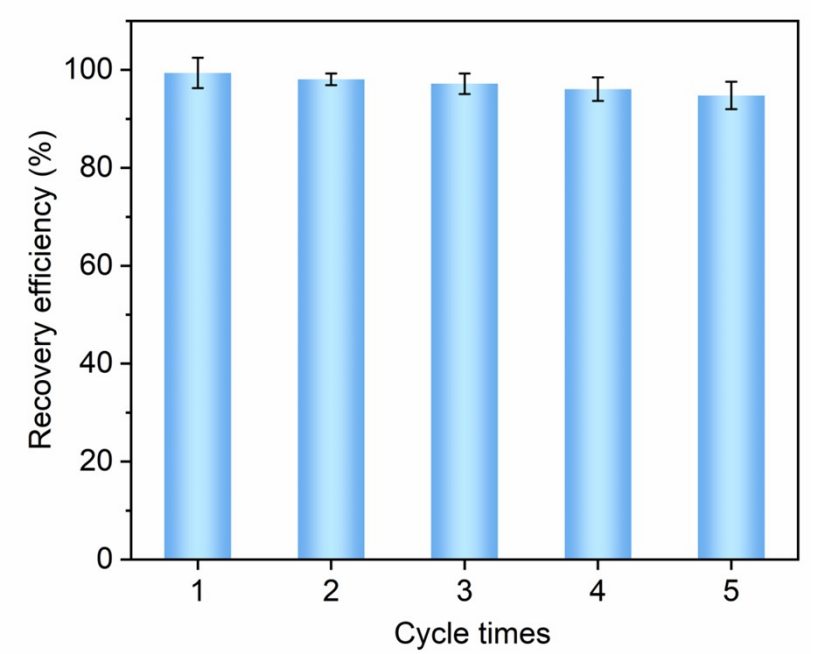

Fig. S15 Recycling experiment of MIPAF-25% in H_2O_2 solution (0.01 M).

After five consecutive cycles, the adsorption capacity of MIPAF-25% in H_2O_2 solution decreased by 5.2%.

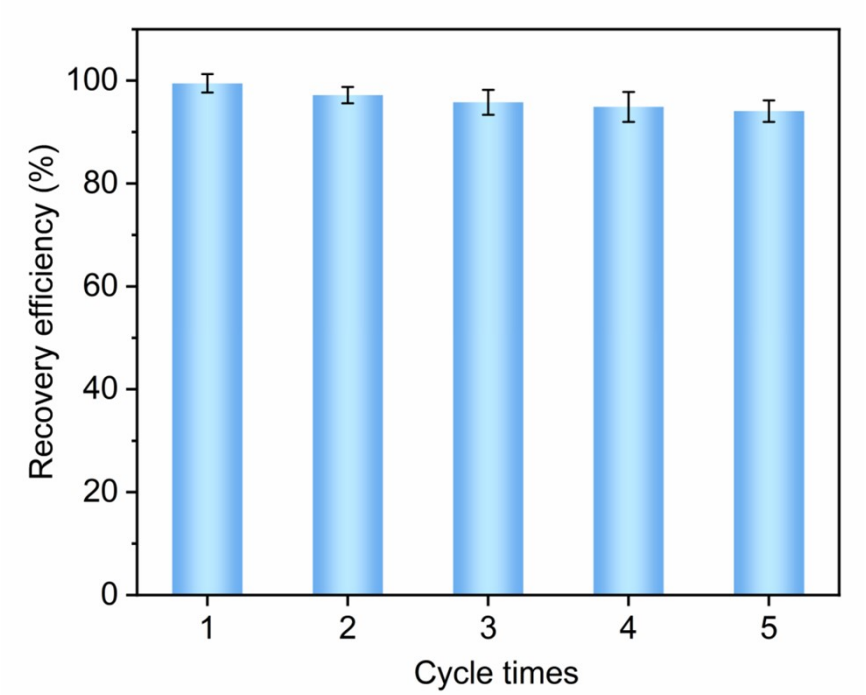

Fig. S16 Recycling experiment of MIPAF-25% in FAS solution (0.01 M).

After five consecutive cycles, the adsorption capacity of MIPAF-25% in FAS solution decreased by 5.9%.

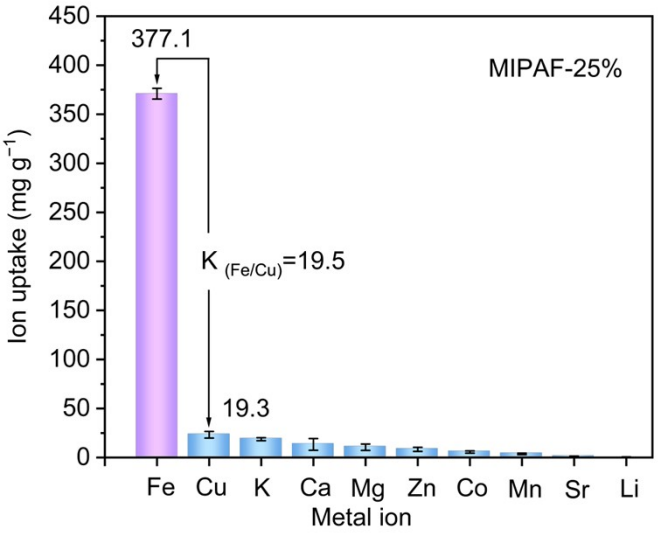

Fig. S17 Selectivity of MIPAF-25% in iron ion solutions containing different competing metal ions.

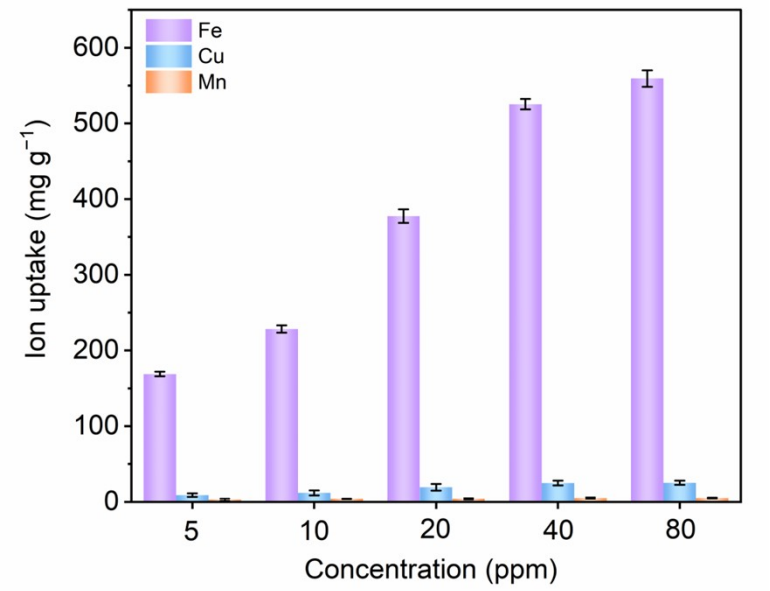

Fig. S18 Selectivity of MIPAF-25% towards Cu and Mn in solutions of varying iron ion concentrations.

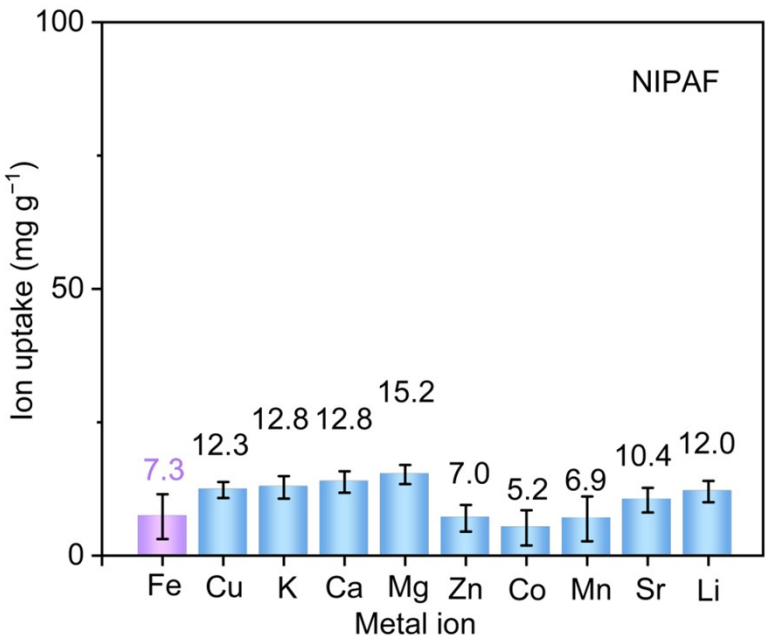

Fig. S19 Selectivity of non-imprinted PAF sample (NIPAF) in iron ion solutions containing different competing metal ions.

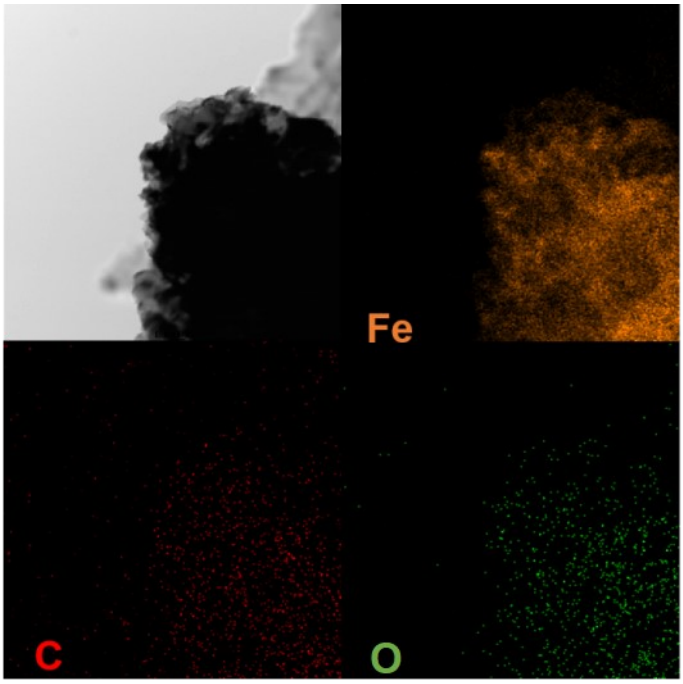

Fig. S20 Energy-dispersive X-ray spectroscopy (EDS) mapping images of MIPAF-25%.

Table S1. BET surface areas and pore sizes of MIPAF-0% and MIPAF-25%

Sample	S_{BET} (mg g^{-1})	Pore size (nm)
MIPAF-0%	799	0.52
MIPAF-25%	540	1.03

Table S2. Kinetic parameters by nonlinear fitting of the material in a 20 ppm iron ion solution

Material	*Pseudo−first−order* model		*Pseudo−second−order* model	
	k_1 (min^{-1})	R^2	k_2 ($mg\ g^{-1}\ min^{-1}$)	R^2
MIPAF-25%	0.0026	0.8733	0.0159	0.9998

Table S3. Adsorption rate constants for MIPAF-25%, MIPAF-30% and MIPAF-40%

Material	k_2 (mg g^{-1} min^{-1})
MIPAF-25%	0.01590
MIPAF-30%	0.00605
MIPAF-40%	0.01880

Table S4. Nonlinear fitting results a 20 ppm iron ion solution

Material	*Langmuir isotherm*		*Freundlich isotherm*	
	b (L min^{-1})	R^2	*n*	R^2
MIPAF-25%	0.0658	0.9811	0.3320	0.9477

Table S5. Selectivity of MIPAF-25% towards Cu and Mn in solutions of varying iron ion concentrations

Concentration	Ion uptake Fe	Ion uptake Cu	Ion uptake Mn	Selectivity ($K_{Fe/Cu}$)	Selectivity ($K_{Fe/Mn}$)
5 ppm	168.8	8.8	0.7	19.2	241.1
10 ppm	228.3	11.8	0.9	19.3	253.7
20 ppm	377.5	19.3	1.4	19.6	270.0
40 ppm	525.4	24.9	1.9	21.1	276.5
80 ppm	559.3	25.2	2.0	22.2	279.7

Table S6. Comparison of selectivity with other adsorbents

Material	Selectivity ($K_{Fe/Cu}$)
MIPAFs	19.5
TPP	10.1
4(1h)-pyridinone	9.2
Deferiprone	8.2
Imprinted microsphere	8.0
Methanesulfonic acid	7.3
Deferasirox	6.9
PMAA	3.0
Multidentate silica gel	1.7

The adsorption properties of all adsorbent materials were obtained from parallel experiments with reference to MIPAF-25%.

Table S7. Comparison of extraction performance with other adsorbents

Material	Capacity (mg g^{-1})	Ref.
MIPAFs	378.0	Our work
HEMA-MAGA	206.4	1
AA-Fe-IIP	114.3	2
Fe-imprinted clay	78.5	3
Acrylic acid-Fe-IIP	62.4	4
MAA-Fe-IIP	40.4	5
Cyanato-imprinted	36.9	6
Imprinted beads	29.2	7
IIP-PMAA	26.8	8
Multidentate silica gel	14.4	9
CMCS	250.0	10
Immobilized BT	106.3	11
Activated carbon	50.0	12
D001	11.7	13
D412	20.5	14
D468	2.3	15

References

1. V. Karakoc, *Hace J. B. Chem*., 2020, **48**, 319-331.
2. G. Zhu, H. Tang, H. Zhang, L. Pei, P. Zhou, Y. Shi, Z. Cai, H. Xu and Y. Zhang, *Hydrometallurgy*., 2019, **186**, 105-114.
3. M. Karabork, A. Ersoz, A. Denizli and R. Say, *Ind. Eng. Chem. Res.*, 2008, **47**, 2258.
4. S. Kumar and M. Shraddha, *J Sci. Ind. Res.*, 2010, **69**, 767-772.
5. M. Roushani, T. Beygi and Z. Saedi, *Spec*. *Acta*. *Mol*. *B*. *Spec*., 2016, **153**, 637-644.
6. H. Shen, T. Liu, and J. Li, *J*. *Shenyang Univ*. *Chem*. *Tech*., 2018, **32**, 289-293.
7. M. Karabork, A. Ersoz, E. Birlik and R. Say, *Hacet*. *J*. *B*. *Chem*., 2007, **35**, 135-142.
8. C. Hu, L. Mao, X. Hu, and Y. Meng, *J*. *Func*. *Mater*., 2018, **49**, 3087-3091.
9. P. Chen, R. Li, and B. Chen, *Chin*. *J*. *Anal*. *Chem*., 2022, **50**, 300-309.
10. X. Wang, H. Jiang, H. Tian and G. Xuan, *Chem*. *B*., 2009, **26**, 30-33.
11. Y. Shen, W. Liu, Y. Li, C. Ma, Y. Li, W. Liu, Y. Liao and B Mao, *J*. *Sichuan Normal Univ*., 2016, **39**, 705-710.
12. X. Zheng, *Chem*. *Ind*. *Times*., 2019, **33**, 6-919.
13. X. Duan, W. Wang, C. Wang, W. Feng and Q. Liu, *Ind*. *Water Wastewater*, 2011, **42**, 64-67.
14. L. Yang, L. Li, S. Huang, M. Wu and M. Liu, *Chin*. *J*. *Rrea Metlas*., 2009, **33**, 401-405.
15. W. Feng, W. Wang, C. Wang and J. Hu, *J*. *Wuhan Inst*. *Tech*. 2021, **32**, 8-11.